Aerosol and Air Quality Research, 18: 254–269, 2018

ISSN: 1680-8584 print / 2071-1409 online
doi: 10.4209/aaqr.2017.01.0021

A Case Study on Fog/Low Stratus Occurrence at Las Lomitas, Atacama Desert (Chile) as a Water Source for Biological Soil Crusts

Lukas W. Lehnert[1*], Boris Thies[1], Katja Trachte[1,2], Sebastian Achilles[1], Pablo Osses[3], Karen Baumann[4], Jakob Schmidt[1], Elena Samolov[5], Patrick Jung[6], Peter Leinweber[4], Ulf Karsten[5], Burkhard Büdel[6], Jörg Bendix[1]

[1] *Faculty of Geography, Philipps-University of Marburg, 35037 Marburg, Germany*
[2] *Department of Geography, Ruhr-University of Bochum, 44780 Bochum, Germany*
[3] *Instituto de Geografia, Pontificia Universidad Catolica de Chile, Santiago de Chile, Chile*
[4] *Faculty of Agricultural and Environmental Sciences, Soil Science, Rostock University, 18051 Rostock, Germany*
[5] *Institute of Biological Sciences, Applied Ecology and Phycology, Rostock University, 18051 Rostock, Germany*
[6] *Plant Ecology and Systematics, University of Kaiserslautern, 67663 Kaiserslautern, Germany*

ABSTRACT

The Atacama Desert is well known for the high occurrence of large-scale fog (spatial extents: hundreds of kilometers) emerging as low stratus (LST) decks over the Pacific Ocean. By contrast, the small-scale and heterogeneous occurrence of small-scale fog (hundreds of meters) particularly during summers is widely unconsidered. However, these events are important for the local vegetation and particularly for the biological soil crusts (BSC) that are widely distributed in this extreme ecosystem. Consequently, a case study in a typical fog oasis in the Pan de Azúcar National Park was conducted to test the feasibility combining field measurements, drone profiling, remote sensing and numerical modeling (i) to investigate fog-type specific differences regarding dynamics, physical properties and formation, (ii) to test the applicability of remote sensing technology for fog monitoring based on existing low-resolution and a proposed new high-resolution product and (iii) to estimate the related fog water input to BSCs. Two types of fog were observed. The well-known fog/LST deck emerging from the Pacific Ocean with high water path and large spatial extent was the first type. Fog of the second type was patchier, small-scale and not necessarily connected to the LST over the ocean. Instead, fog formation of the second type was related to thermal breeze systems, which produced shallow clouds containing less water than those of type 1. In general, such small-scale fog events were not captured well by existing remote sensing products but could be detected with the proposed new high-resolution product which provided promising results. Both fog types were important water resources for the BSCs, with approximately 8% to 24% of the fog water flux available to the BSCs at the surface. The results indicated the feasibility of the proposed methods' pool to estimate the water budget of BSCs with a high spatial resolution in the future.

Keywords: Orographic fog; Landsat; WRF-modeling; Biological soil crusts; Vertical fog droplet spectra.

INTRODUCTION

Formed by living organisms, biological soil crusts (BSC) and their by-products create a surface soil layer of inorganic particles bound together by organic materials (e.g., Belnap and Lange, 2001). With other microorganisms such as heterotrophic bacteria, fungi and macroscopic lichens, cyanobacteria and algae represent the most important phototrophic component of BSCs (Elbert *et al.*, 2012). On a global scale, BSCs form the most productive microbial biomass under extreme environmental conditions such as in drylands. Therefore, BSCs can be characterized as "ecosystem-engineers" (e.g., Bowker *et al.*, 2006) that have important, multi-functional ecological roles in primary production, nutrient and hydrological cycles, mineralization, dust trapping, chemical weathering and stabilization of soils (e.g., Castillo-Monroy *et al.*, 2010). In a recent review, the important ecological role of BSCs in global carbon (C) assimilation (approximately 7% of terrestrial vegetation) and N fixation (approximately 50% of terrestrial biological N fixation) (Elbert *et al.*, 2012) was clearly established, although only a little is known about their role in the biogeochemical cycle of phosphorus. This particularly holds for arid areas such as the Atacama Desert in northern Chile because of the few studies on cryptogamic organisms

[*]Corresponding author.
E-mail address: lukas.lehnert@staff.uni-marburg.de

in this area. The prerequisite for any C-, P- and N-fixation is the availability of moisture. In desert regions such as the Namib, the Atacama, and the Negev-Desert, these important biotic crusts are assumed to rely on the small amount of water supplied by fog water deposition or nocturnal dew formation (Lange 1980; Lange and Redon 1983; Lange *et al.*, 1994). In the Namib Desert, depending on the species, 0.13 to 0.26 mm of water is sufficient for the activation of BSCs (Lange *et al.*, 1994). To assess the spatial occurrence of BSCs and therefore their potential contribution to C-, P- and N- cycles, the spatio-temporal availability of fog water must be known at high spatial resolution. However, to date, this information has not been determined for the Atacama Desert.

Several studies on fog occurrence and water availability have been conducted at several sites in the Atacama Desert. Cereceda and Schemenauer (1991) showed that fog frequency is generally highest in the coastal areas, peaking between 35° and 40°S, with approximately 38 fog days per year. However, frequencies with 189 days of fog (+84 days with patchy fog at approximately 900 m a.s.l.) are particularly high at the more elevated parts of the coast (Cereceda and Schemenauer, 1991). Requiring dense networks of observations (Schemenauer *et al.*, 1987), fog water availability in the Atacama Desert is a complex function of the topography, seasonal wind field and trade inversion height, which partly lead to patchy small-scale fog oases. Consequently, the positive effect of fog water on vegetation growth in space and time is also complex and non-linear (Borthagaray *et al.*, 2010, Muenchow *et al.*, 2013). The highest fog frequencies occur in austral winter when the eastern Pacific stratus deck is well-developed, intruding into the coastal areas where the availability of fog water depends on the advection process and the height of the stratus base relative to the altitude (Cereceda *et al.*, 2008a; Schulz *et al.*, 2011). In the other seasons, fog is less frequent and patchier, partly related to nocturnal radiation and orographic fog formation in specific topographic situations (Cereceda *et al.*, 2002; Sträter *et al.*, 2010). The primary fog water input is from June to October, with a peak in September (Cereceda *et al.*, 2008a). In the water supply for vegetation, fog water can significantly complement (or even replace) rainfall, particularly in the arid to semi-arid regions of Chile, and is elevated during La Niña and depleted during El Niño years (Garreaud *et al.*, 2008). For example, in the very dry areas receiving 0.8 mm annual rainfall, fog water deposition to *Tillandsia* species was 25 mm per year (Westbeld *et al.*, 2009). With fog collectors mimicking areas of high aerodynamic resistance, fog water input can reach values > 20 mm per day (Cereceda *et al.*, 2004). However, the spatial extent of fog and fog water deposition on a local scale are widely unknown particularly regarding the availability of fog water to the tiny BSCs. In a first study that focused on the regional scale based on an analysis of GOES weather satellite data with 4 km spatial resolution, low stratus (LST) extension increased with increasing trade inversion height, but to date, ground contact, fog water content and deposition have not been retrieved from GOES data (Cereceda *et al.*, 2008a). Therefore, the small-scale fog events as described by Cereceda *et al.* (2002) and Sträter *et al.* (2010) are likely not captured with existing remote sensing products. Consequently, no spatially explicit information is available on fog water input at higher spatial resolutions that might capture the specific situations in the small-scale fog oases.

The focus of the current case-study was to unveil the fog dynamics in austral autumn in a typical fog oasis (Las Lomitas) of Pan de Azúcar National Park, Atacama Desert. For this study, ground measurements, profiling techniques, numerical modeling and high resolution satellite retrievals were combined (i) to investigate fog-type specific differences regarding (a) dynamics, (b) physical properties and (c) formation, (ii) to test the applicability of remote sensing technology for fog monitoring based on existing low-resolution and a proposed new high-resolution product, and (iii) to estimate the related ecosystem fog water input to BSCs.

STUDY AREA AND METHODS

Study Area

Pan de Azúcar National Park is located between 25°53′ to 26°15′S and 70°29′ to 70°40′W along the Pacific coast in Chile (Figs. 1(a) and 1(b)). The area is included in the southern part of the Atacama Desert. A narrow pediment close to the coast characterizes the local topography, and inland, a steep mountain ridge emerges reaching altitudes up to 850 m a.s.l. (Fig. 1(f)). After this first mountain ridge, the terrain descends slightly to altitudes between 400 and 700 m a.s.l. Our meteorological stations were located in a local fog oasis in the national park called Las Lomitas, which is situated in the northern part close to the coastal crest of the first mountain ridge. This first mountain ridge is concavely formed around Las Lomitas.

Rundel *et al.* (1996) and Thompson *et al.* (2003) describe the overall climate of the park area. Annual rainfall is less than 13 mm but higher totals and extreme precipitation (7.5 mm per two days) can occur occasionally during El Niño years. Lower temperatures are registered in austral winter (July) when the absolute minimum can drop to below 3°C at night (daily maximum at approximately 17°C, average ≈13°C), whereas the highest temperatures occur in austral summer (January), with daily maxima occasionally exceeding 26°C (minimum approximately 15°C, daily average ≈20°C). Lapse rate is stable over the year with approximately 0.65 K/100 m. Typical air humidity ranges from 80% to 85% at night and from 60% to 70% during daylight. Vapor pressure deficit (VPD) is highest during austral summer (at 0.8 to 1.0 kPa levels) but generally lower than that in other desert systems. Wind direction is stable over the year with a predominant advection from the sea from the WNW-direction (286°) and smaller portions from the east in austral autumn and winter which characterizes nocturnal drier and colder katabatic drainage flows. During daylight a well-developed onshore breeze emerges, concomitant with high humidity, a stable adiabatic lapse rate, and a vertical inversion layer. The stable stratification in the inversion layer is related to the cold upwelling of the Humboldt Current

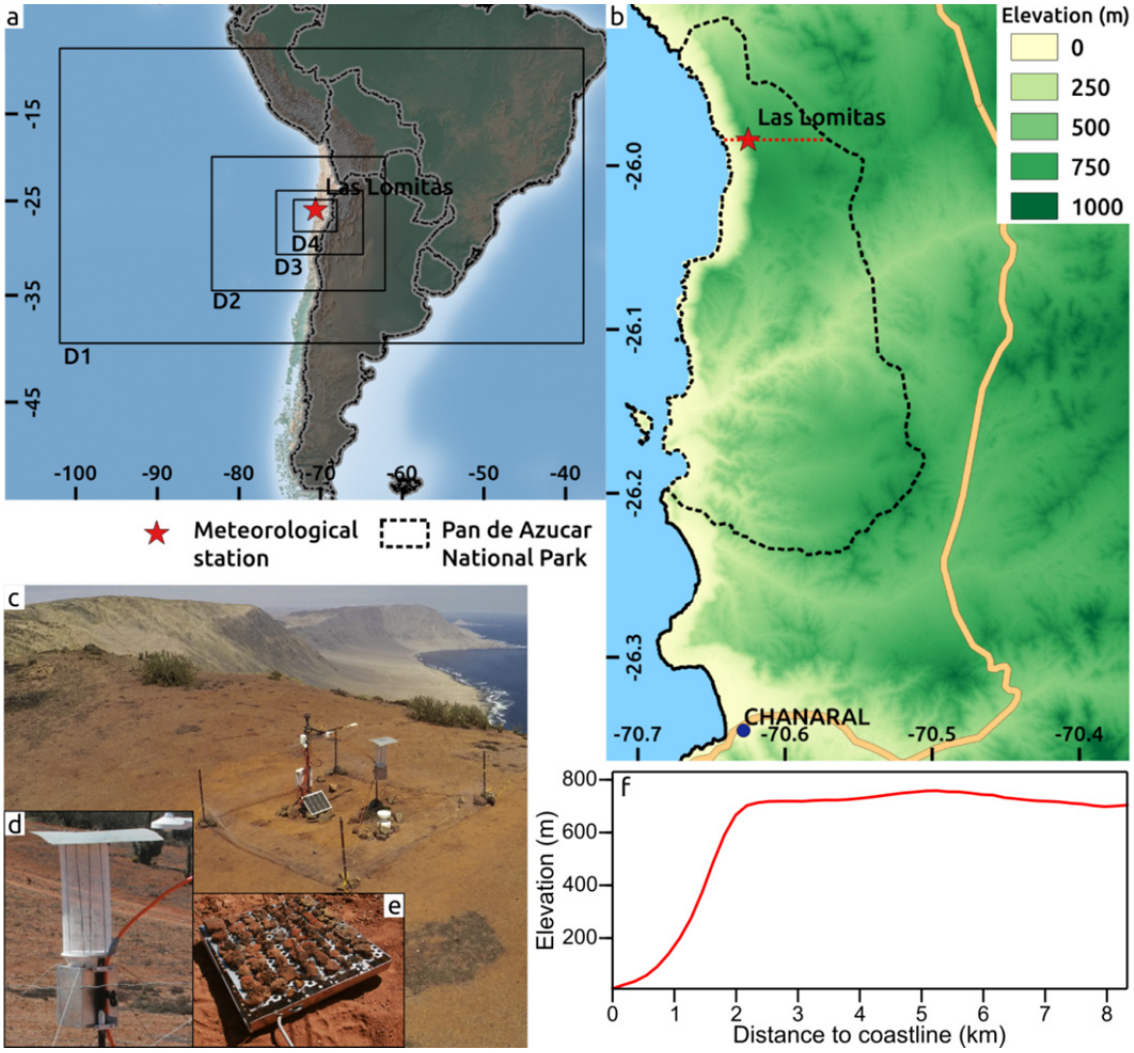

Fig. 1. Map of Pan de Azúcar National Park with the locations of the meteorological stations (a, b). The rectangles in (a) depict the four different nested domains of the WRF-model. Photographs are of the main station at the ridge (c), the fog collector (d) and the biocrust scale (e). The cross section (f) showing the altitudinal profile at the meteorological stations is depicted with red dotted lines in the map (b).

and the clear influence of the South Pacific Anticyclone, which is responsible for the thick stratus deck covering large areas offshore the park. Fog, locally termed Camanchaca, mostly affects the coastal areas (such as Las Lomitas) but rarely extends further inland along the fluvial channels interspersed along the coastline. In Las Lomitas, soil moisture on open sites ranges from 7 to 17 vol.-% (Stanton *et al.*, 2014).

Cacti and shrubs dominate the vegetation at Las Lomitas, particularly the cactus *Eulychna saint-piena* and several shrubs of the genus *Euphorbia*. From heavy rains the year before our visit, several herbal plants were observed but were in a state of disintegration and could not be identified taxonomically. BSCs were constantly present with coverages between 30% at the front ridge and 21% on the leeward side. The green algal lichens of the genera *Acarospora*, *Caloplaca*, *Placidium* and *Rinodina* dominated the BSCs, with various representatives of Chlorophyta (e.g., *Elliptochloris*, *Chlorococcum*, *Diplosphaera*), Streptophyta (e.g., *Klebsormidium*) and filamentous Cyanobacteria (e.g., *Nostoc, Microcoleus*).

Methods

To determine the types of spatio-temporal fog dynamics, to test the applicability of remote sensing for fog monitoring and to estimate the related ecosystem fog water input for biological soil crusts, ground measurements, profiling techniques, numerical modeling and high-resolution satellite retrievals were combined (Fig. 2). Ground measurements were conducted in March 2016, whereas several time periods of remote sensing data were analyzed depending on the availability of data, as stated below.

Automatic Weather Stations

Two automatic weather stations were installed in March 2016 at Las Lomitas in Pan de Azúcar National Park. The first station (termed "main station" in the following) was located close to the mountain ridge at 740 m a.s.l. (Fig. 1(c)).

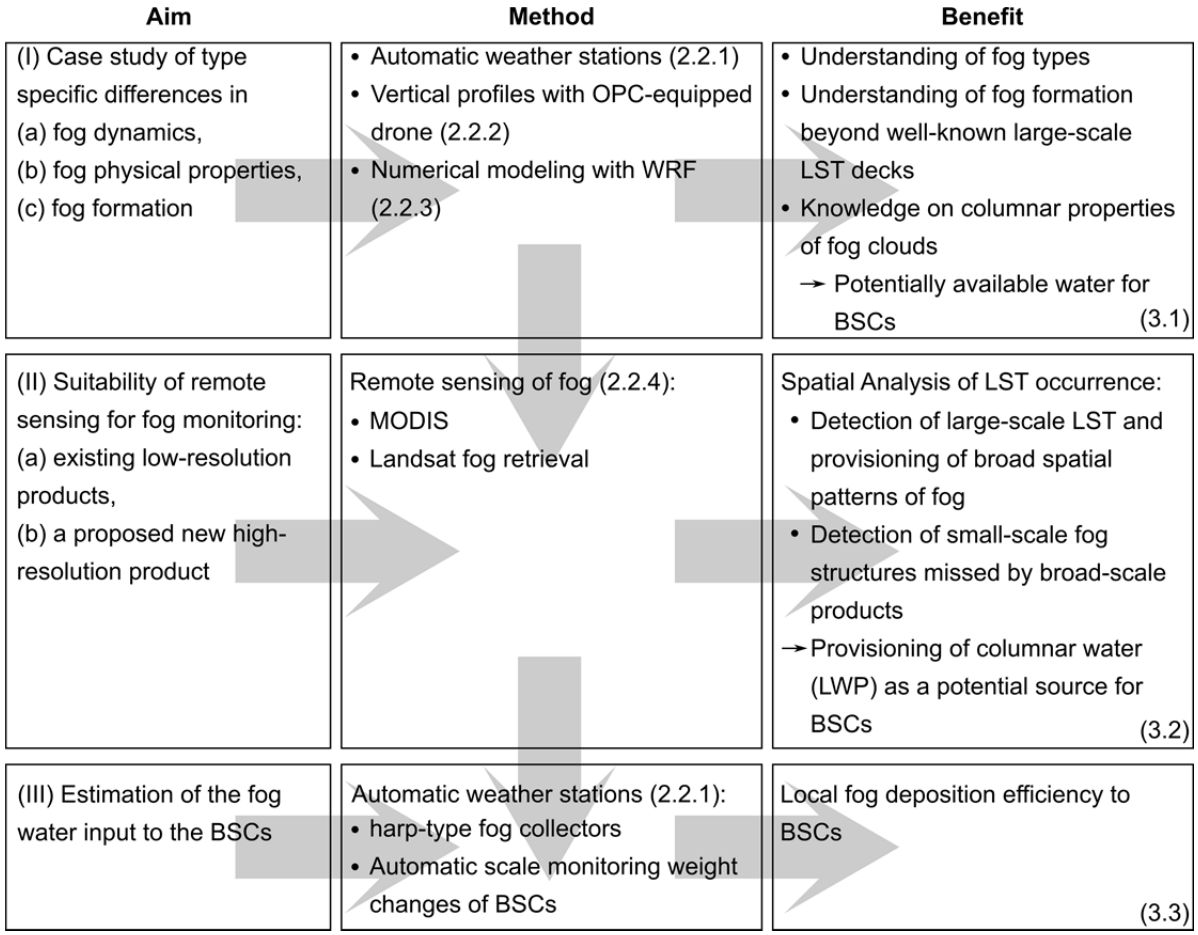

Fig. 2. Flowchart of the methodology. Roman numbers in the first column refer to aims stated in the text. Arabic numbers in the second and third column reference respective methods' and results' sections, respectively. Optical particle counter and low stratus are abbreviated as OPC and LST.

The second station ("remote station") was approximately 250 m farther inland. Both stations were equipped with standard sensors measuring wind speed, wind direction, surface and air temperatures, and relative humidity.

To measure fog water deposition, both stations had cylindrical ("harp"-type) fog collectors (Fig. 1(d)). Compared with standard fog collectors (Schemenauer and Cereceda 1994), the harp-type has the advantage that the sampling effort is not affected by the wind direction. The collectors were designed according to Falconer and Falconer (1980). We used Teflon strings with a diameter of 0.25 mm. The harp encompassed two rows, each with 240 strips. The diameter of the outer and inner rows was 200 and 196 mm, respectively. The height of the strips was 480 mm for a total area of collecting surface of 96×10^{-3} m^2. The water was collected in a bottle and was automatically weighted at a time interval of 1 minute with a resolution of 7.32 mg. If the bottle is full, it is automatically drained. The mass of the water was converted to fog water flux (f) using the following equation:

$$f_t = \frac{\Delta m}{A \rho \Delta t}, \quad (1)$$

where Δm is the mass change of the bottle between two measurements, A is the collection surface of the collector (96×10^{-3} m^2) and ρ is the density of water at 20°C (0.998 kg L^{-1}). The sampling interval ($t_i - t_{i-1}$) at both stations was set to 5 minutes. Both collectors have been installed 1.5 m above ground.

Only a small proportion of the fog water collected by the fog collectors was assumed to be available to the BSCs, primarily because of the following: (i) the most likely low settlement rate of droplets due to relatively high wind speeds and (ii) the nearly negligible aerodynamic resistance of the BSCs on the ground. To quantify the proportion of water that was available to the BSCs in relation to the fog water captured by the fog gauge, a scale was installed (Fig. 1(e)). The scale surface was 25 × 25 cm and was covered with BSC and sufficient soil to ensure that the BSC could survive over a longer time. The scale measured the weight of the BSC and the soil at 5 minute intervals. By relating the changes in weight of the BSC to the collected fog water, the sampling efficiency of a soil surface with BSC was estimated.

Vertical Physical Properties of Fog

Between March 14 and 16, 2016, LST microphysics were

measured over time and along vertical profiles in the field. For the vertical profiles, a drone equipped with an optical particle counter (OPC, Droplet Measurement Technologies, Boulder, Colorado, USA) was used. The instrument is a custom-build model but comparable to the newer version CDP-2. It counts the droplets with diameters between 2 μm and 50 μm (30 size classes) in the air masses constantly pumped through the device. The flights were conducted under foggy conditions at ground. First, the drone climbed to the maximum flight altitude of 250 m. Then, the altitude was stepwise reduced by 25 m until the drone reached the surface. At each 25-m-altitude level, OPC-measurements were conducted for 30 sec. Because the instrument tended to underestimate drop counts, an empirical correction was applied based on visibility data simultaneously recorded with a VPF-730 Present Weather Sensor (Guyot *et al.*, 2015). The VPF-730 is a visibility and present weather sensor manufactured by Bristol Industrial and Research Associates Limited Company, Portishead, Bristol, UK, that determines the extinction coefficient of a specific volume of air using a forward scattering meter. Both instruments recorded data simultaneously over several hours. Then, a linear regression model was fitted between extinction coefficient estimates of the VPF-730 and the OPC to derive a correction coefficient for the OPC-data (Guyot *et al.*, 2015). The corrected drop counts were averaged over each 30 sec measurement interval at each altitude level. Using the averaged drop size spectra, the liquid water content was calculated according to Egli *et al.* (2015).

Numerical Modeling

The Weather Research and Forecasting (WRF) model (Skamarock *et al.*, 2008) was used to investigate underlying processes and dynamics in fog development. WRF is a fully compressible, non-hydrostatic grid-box model with a terrain-following vertical coordinate system. The model was run in a two-way nesting mode with 4 nests: the outer domain had 155 grid points in east-west and 105 in north-south directions with a grid size of 36 km; Domain 2 had 163 by 136 (12 km), and domain 3 253 by 193 grid points with a spatial resolution of 4 km. To capture the topographical features and, thus, slope driven circulation patterns likely inducing fog formation, the inner domain was set to 401 by 401 grid points and a grid size of 1 km focusing on Pan de Azúcar National Park (see Fig. 1). In the vertical direction, 51 layers were applied, with most layers arranged in the lower troposphere. The simulations were driven by the ERA-Interim data (Dee *et al.*, 2001), and the surface properties (land coverage and topography) were described by the USGS 24 land categories and the GTOPO30 terrain data. The parameterization schemes used are summarized in Table 1.

Remote Sensing of LST/Fog

Satellite data were used to analyze the spatial pattern of low cloud frequencies at Las Lomitas and the surrounding coast of Pan de Azúcar National Park. Color composites of low resolution GOES data provide information on the diurnal course of low stratus decks in the greater vicinity of the study area. As medium resolution data, a time series of the MODIS (Moderate Resolution Imaging Spectroradiometer) cloud product (MOD35) was analyzed using all available scenes acquired between 2011 and 2014. The data featured a spatial resolution of 1 km with two satellite overpasses per day between 1100 and 1300 local time. The cloud product is the result of several tests with yes/no decisions. The presence of low clouds in each available image was determined using the result of the low cloud test, which is based on the difference in the 11 and 3.6 micron channels (Ackerman *et al.*, 1998). Low cloud frequency for each pixel was calculated as the number of overpasses with low clouds divided by the total number of overpasses.

To obtain information on fog frequencies with higher spatial resolution, Landsat 8 data were analyzed. For information on cloud properties such as cloud optical depth, the NOAA-AVHRR approach of Bendix (1995) was adjusted for the use with Landsat 8 data. The approach is based on the difference in the albedo between cloudy (ρ) and non-cloudy days (ρ_s) accounting for spatial changes in the land surface albedo that particularly influence the cloud top albedo (ρ_c) of optically thin clouds (Dedieu *et al.*, 1987):

$$\rho_c = \frac{\rho(\lambda) - \rho_s(\lambda)}{1 + \rho(\lambda)\rho_s(\lambda) - 2\rho_s(\lambda)} \quad (2)$$

Therefore, at least two images are required: one cloud free image as a reference and one cloudy image. The two images were atmospherically corrected using a modified and extended version of the 6S-Code (Vermote *et al.*, 1997; for the modifications see Curatola Fernández *et al.*, 2015). To properly parameterize the atmosphere at the time of overpass, temperature, humidity and pressure profiles from NCAR reanalysis data were used (Kalnay *et al.*, 1996). Ozone and aerosol contents were extracted from Aura OMI data (Dobber *et al.*, 2006; Levelt *et al.*, 2006). The influence of the topography on the surface albedo values of the cloud-free scene was eliminated applying a statistical topographic correction method proposed by Teillet *et al.* (1982). For elevation data, the Aster digital elevation model data with 30 m spatial resolution were used (Tachikawa *et al.*, 2011)

Table 1. WRF parameterization schemes considered for the case study and respective references.

Physics	Scheme	Reference
Cumulus convection	Kain-Fritsch	Kain (2004)
Microphysics	Thompson	Thompson *et al.* (2004)
Planetary boundary layer	Yonsei University	Hong *et al.* (2006)
Land surface model	Noah Surface Model	Tewari *et al.* (2004)

and projected onto the Landsat grid applying bi-linear resampling. The cloud top albedo (ρ_c) was then used to estimate cloud optical depth according to Stephens (1978):

$$\delta(\mu_0) = \frac{\rho_c \mu_0}{(1-\rho_c)\beta(\mu_0)}, \quad (3)$$

where μ_0 is the cosine of the solar zenith angle and β is the backscattered fraction of radiation taken from a look-up table. Liquid water path (LWP, in g m^{-2}) was then calculated using an empirical transfer function (Stephens, 1978; Kriebel, 1998):

$$LWP = 10^{(0.5454\delta)^{0.254}} \quad (4)$$

RESULTS AND DISCUSSION

Fog Dynamics, Fog Physical Properties, and Fog Formation

The average daily course of fog water input at the main station collected with the cylindrical fog collectors showed different shapes in March and April (Fig. 3). In March, the highest values occurred in the noon to afternoon hours, whereas only a slightly higher fog water input occurred at night in April. At the remote station, the noon–afternoon peak also occurred in April. The average daily fog water flux is highly consistent with values found at Alto Patache north of Las Lomitas by Cereceda *et al.* (2008a). With 2.53 L m^{-2} (remote station: 3.98 L m^{-2}) in March versus 5.54 L m^{-2} (remote station: 6.58 L m^{-2}) in April, the observation period clearly marked the transition from austral autumn with low fog water to austral winter with clearly higher values of fog water input (Cereceda *et al.*, 2008a).

The liquid water content (LWC) profiles recorded by the drone system at Las Lomitas were taken during a period of emerging fog patches. The profiles showed that the geometrical thickness was less than 250 m and the highest water density occurred at an altitude 100 m above ground (Fig. 4). Although, the profiles indicated that a large proportion of the LWP was not influencing the vegetation at the ground, the information is important for any satellite-based fog observation (see Section 3.2), because the estimation of the LWC at ground from the LWP is a crucial task (Bendix *et al.*, 2005; Li *et al.*, 2008; Cermak and Bendix, 2011). The average LWC measured with the OPC on-board the drone ranged in the order of radiation fog in Germany (0.01–0.13 g m^{-3}, Bendix 1995), and the LWP was 14.84 g m^{-2}. The droplet spectrum showed generally very small droplets, with the highest mode diameter approximately 8 μm at the LST top. The mode diameter decreased toward the ground at which the higher temperatures might increase the VPD, leading to droplet evaporation. Small mode diameters between 4–8 μm are typical for ground fog and the fog formation stage (Tampieri and Tomasi, 1976).

To understand fog formation, a WRF simulation was conducted for a fog event on April 25, 2016 (Fig. 5). The model results indicated that a fog layer formed on the upper cliff of Las Lomitas beginning in the night, showing the highest cloud water amount between elevations of 500 and 750 m a.s.l. Fog formation is related to easterly low level airflow at ground from the inland Atacama Desert, which indicates thermally induced katabatic flows from the Andean slopes (Trachte *et al.*, 2010a). The cold air drainage converges with the relative warm moist air masses over the coastal waters advected from the Pacific Ocean leading to lifted condensation (Angelis *et al.*, 2004; Cunningham, 2007; Trachte *et al.*, 2010b). The fog patch was topped by an inversion layer, which started to develop after midnight and intensified after sunrise, typical for orographic fog situations. With sunlight, the breezes system intensified and encroached the area behind the coastal cliff-line, where a constituting sea breeze led to an inland movement of shallow fog formation with considerable water amounts. The fog formation lasted until noon, when the inversion above the cliff dissipated. The absent inversion then led to an uplift of the low clouds accompanied with heavy condensation at the beginning of the condensation process. At 1500, the clouds totally dispersed.

Fog water flux locally collected on April 25, 2016, with the fog sampler began immediately after midnight (Fig. 6(a)). The amount of collected water decreased between 0300 and 0600 and then strongly increased until sunrise. During the day, fog water input was recorded until 1600 with the highest amounts approximately at noon. The inland intrusion as observed by the numerical modeling, particularly along valleys breaching the coastal cliffs, was also apparent in the GOES data presented in Fig. 6(b). The images taken during the night showed that a shallow cloud covered the coastal area that was not connected to the LST deck over the Pacific Ocean. After sunrise, the cloud over the coast enlarged in extent until 1000. After noon, the cloud begun to disappear, confirming the WRF simulation results for both the appearance of clouds and the cloud water content leading to the observed fog water flux collected at the ground.

Remote Sensing of LST/Fog

MODIS monthly LST frequency in the area of Pan de Azúcar National Park showed a clear spatial discrimination between the very frequent stratus deck occurrence over the coastal waters (60–80% LST cover in relation to all satellite overpasses) and the very low frequencies in inland Atacama (0–10%). The sharp decline of LST occurred in the first 2–3 km behind the coastal line, where Las Lomitas was also situated, confirming the results of several previous studies (e.g., Cereceda *et al.*, 2002; Larrain *et al.*, 2002; Cereceda *et al.*, 2008a, b; Garreaud *et al.*, 2008). Behind the coastal line, LST frequency could reach 50% (SON), with the highest extension inland observed in November (Fig. 7). In most months, LST frequency reached approximately 20–60% at the coastline (for March and November see Fig. 7, other months not shown because they show intermediate conditions between the minimum and maximum frequencies in March and November, respectively). However, the subpixel fog that frequently occurred with a spatial extent of less than the 1 km MODIS pixel resolution over the bright desert might not be classified correctly. In this case,

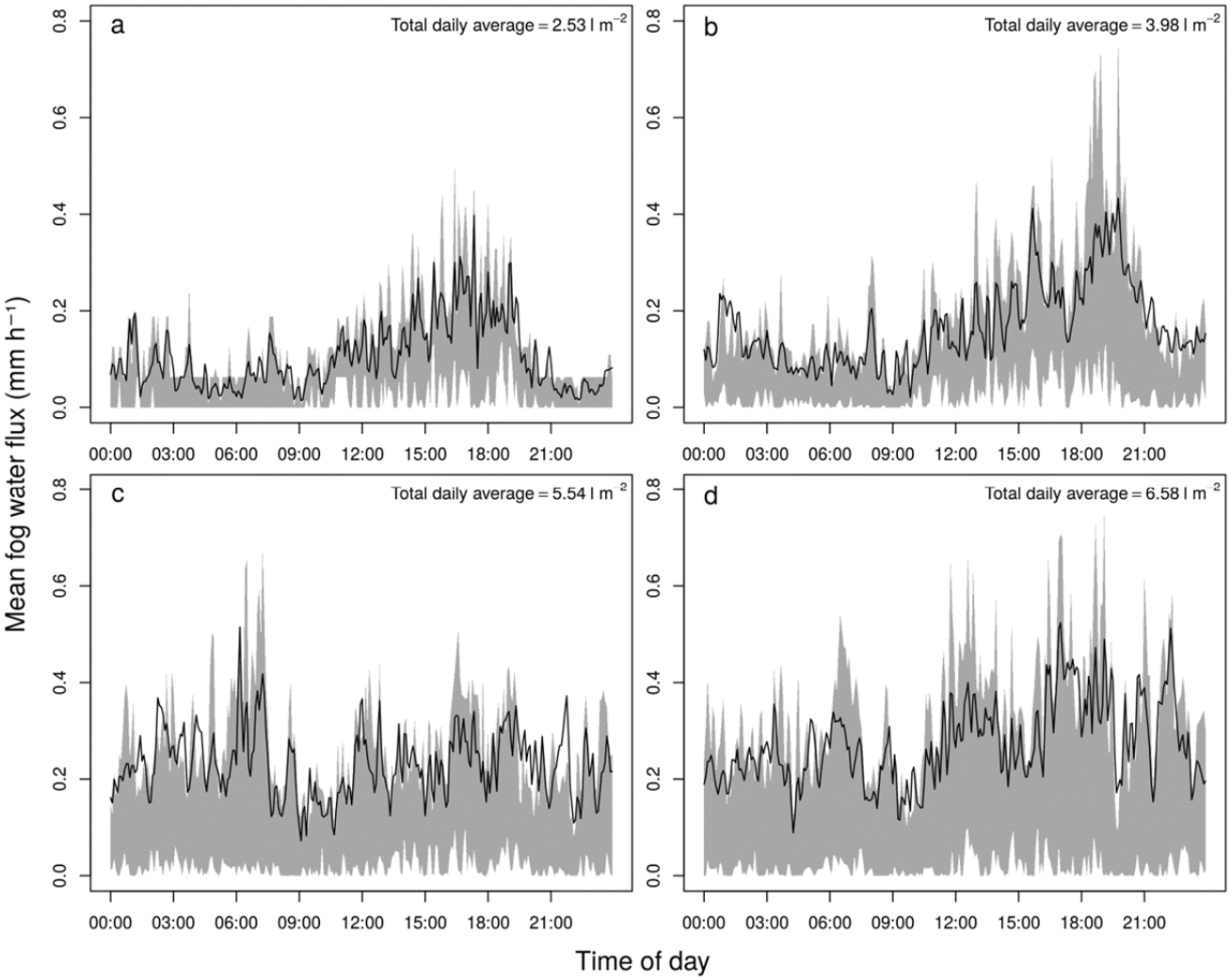

Fig. 3. Average diurnal course of fog water input in March 2016 at the main (a) and the remote station (b) installed at Las Lomitas, Pan de Azúcar National Park. Figures in (c) and (d) depict fog water input in April 2016 at the main and the remote station, respectively. Gray areas denote the inter-quartile ranges. Please note that mean values were highly influenced by single fog events during the respective time of the day when mean lines are close to or outside of the inter-quartile ranges. Fog water fluxes were measured with cylindrical harp-type fog collectors and should not be considered water input at soil surface.

an underestimation of LST occurrence might be possible due to missing LST subpixels (Obregon *et al.*, 2014).

To analyze small-scale structures of fog, high-resolution satellite data are required. Fig. 8 shows two examples of different fog/LST types, which were based on Landsat 8 retrievals. In the image taken on March 10, 2016 the marine stratus deck was clearly located off the coast and the coast itself was just covered by small patches of fog that affected the sites of Las Lomitas if the cloud had ground contact (Fig. 8(a)). Cloud optical depth (COD) and LWP of the fog patches were relatively low (cloud optical depth 3–4, liquid water path 6–12 g m^{-2}), as a result of small vertical extension of the patches at this time (see Section 3.1). The values are clearly lower than average conditions in the mid-latitudes, at which values of cloud optical depth range from 8.5 to 13.6 and LWP is between 30 g m^{-2} and 50 g m^{-2} (Bendix, 2002) but are similar to those of shallow radiation fog layers in this area (COD 0.6–5, LWP 5.6–13.7 g m^{-2}, Bendix, 1995). The range of the LWP estimates is slightly below the OPC-derived value a few days after (14.84 g m^{-2}), indicating that the estimations from the satellite retrieval were consistent with the observations during such small-scale fog events. The fog patch covered the slope and plateau area of the coastal cordillera between 420 and 830 m a.s.l. One month later (April 11, 2016), an extended LST layer off the coast also encroached the coastal area, showing very dense clouds (COD up to 82 and LWP up to 100 g m^{-2}, Fig. 8(b)). These high values are typical for thicker and very moist LST decks originally formed over the coastal Pacific (e.g., Masunaga *et al.*, 2002; Wood and Hartmann, 2006; Zhou *et al.*, 2006). However, only small amounts of horizontal water were recorded at the ground on the day with the full cloud cover (April 11, 2016, Fig. 8(c)). Because average daily wind speed was only 1.81 m s^{-1} (lower than

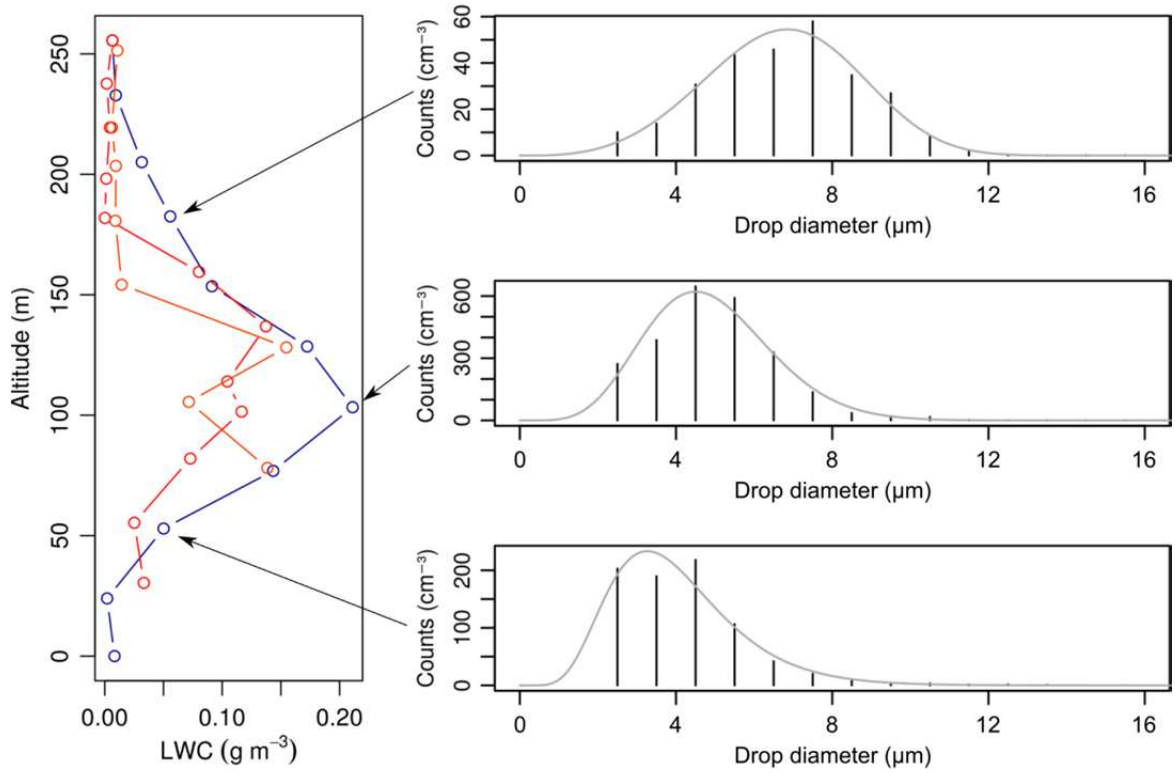

Fig. 4. (Left) Three vertical profiles of fog liquid water content (LWC) recorded on the March 16, 2016 between 1100 and 1130 local time at Las Lomitas, Pan de Azúcar National Park. The altitude was that above ground at the meteorological station (740 m a.s.l.). (Right) Three drop size spectra recorded at different altitudes. Note that the gray line is the modified gamma fit applied to estimate small drop size counts.

the 1st quartile), the cloud base of the LST deck either did not touch the ground or the low air movement dropped the sampling efficiency of the fog collectors, which would both lead to clearly smaller fog water fluxes to the ecosystem. Both explanations are theoretically plausible but could not be tested at the moment because of the lack of data on the cloud base height, for example, from remote sensing, which emphasizes the necessity for high-resolution fog remote sensing products in the Atacama.

Moisture Availability for BSCs Driven by Fog

The time series of mean daily sum of fog water fluxes and water collected by the BSCs is shown in Fig. 9(a). Daily sums of fog water fluxes ranged between 1.3 and 16.6 mm. The water amounts deposited on the BSC scale ranged between 0.4 and 3.6 mm. The highest values of both variables were observed during mid April. A close correlation between the mean daily fog water flux and the water available for the BSC at the soil surface was observed (Fig. 9(b)). Thus, we derived two empirical transfer functions that were used to estimate the water that was available for the BSCs in relation to the fog water flux at Las Lomitas. The first function is a simple linear regression. However, several processes such as the sampling efficiency of the artificial fog collector and the BSC scale and the influence of wind on the BSC-scale may cause the relationship between fog water flux and the water available for the BSC being non-linear. Therefore, we estimated a non-linear transfer function. Both functions revealed similar estimates in the range of our observed values but heavily differed at drier conditions. Based on the linear function, a water amount of 0.77 mm would be expected if now fog occurs. Considering dew as an alternative water source, this value was exceptionally high and seemed to be unrealistic. For instance, Jacobs *et al.* (2000) measured a maximum dew formation of 0.3 mm night^{-1} for a BSC-covered surface in the Negev Desert. For European sand ecosystems covered by BSCs maximum dew formation is reported by 0.18 mm night^{-1} (Fischer *et al.*, 2012). Unfortunately, there are no dew formation measurements for the Atacama (Westbeld *et al.*, 2009). In contrast, the contribution of dew formation to total BSC-available water is lower if a non-linear relationship is assumed (0.32 mm day^{-1}). Although, the high uncertainty of the contribution to dew indicates the need of further research on the water budget of BSCs in the Atacama, the general influence of fog on BSCs could be clearly demonstrated. If a linear relationship is assumed, approximately 11% of the water captured by the artificial fog collector was available for photosynthesis for the BSCs. If the relationship is considered non-linear, between 8% under heavy and 24% under moderate foggy conditions of the collected fog water were available.

CONCLUSION

In this article, *in situ*-meteorological measurements, satellite-based remote sensing observations and numerical

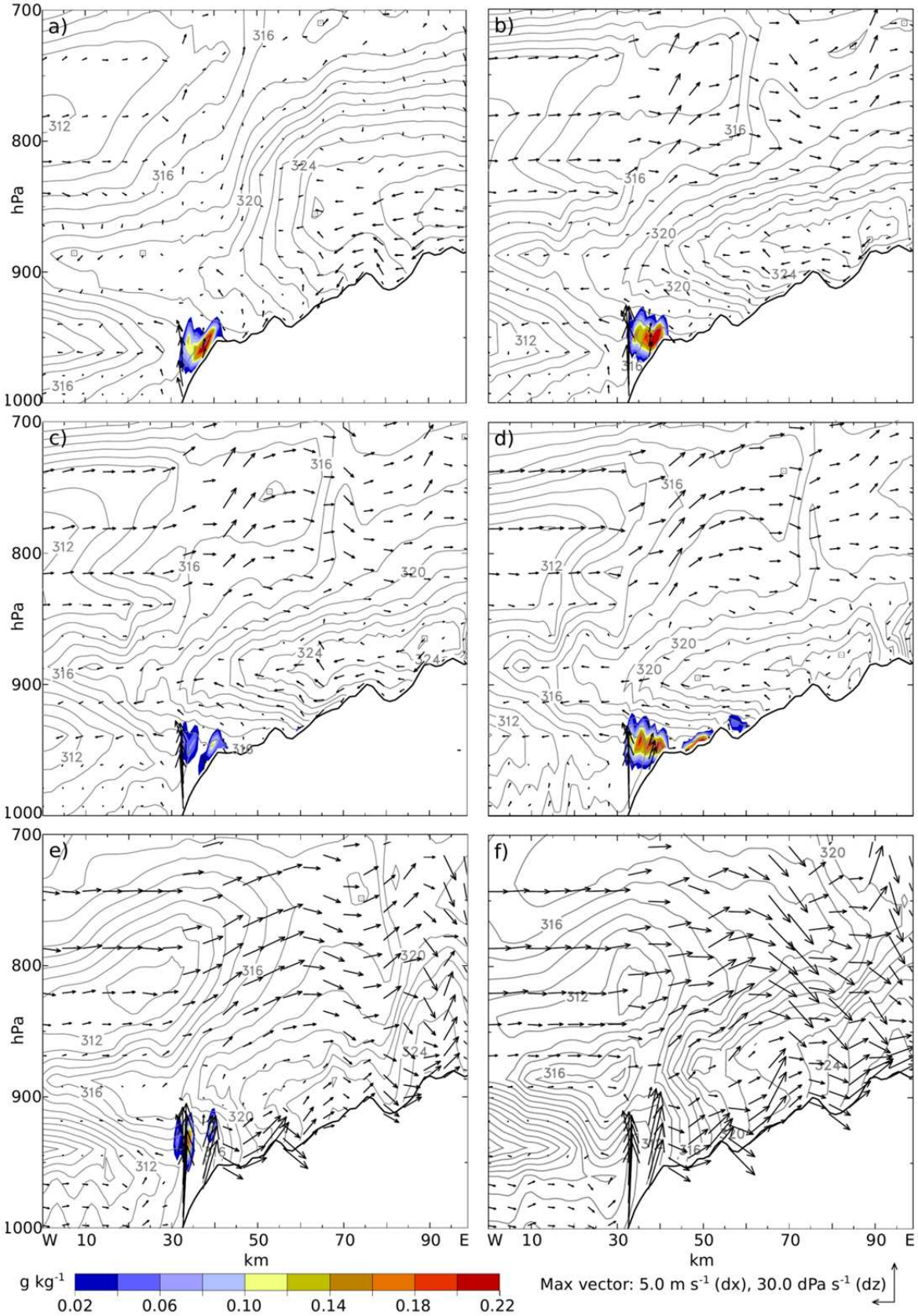

Fig. 5. Vertical cross-section from 70.0° to 71.0°W at 25.9°S of the equivalent-potential temperature (contours, K), the wind field in x-z (uw) directions (vectors, m s^{-1}), and cloud water mixing ratio (shaded, g kg^{-1}) for April 25, 2016, at (a) 0000, (b) 0300, (c) 0700, (d) 1000, (e) 1300 and (f) 1500 local time. The data were based on the predictions of the WRF-model run.

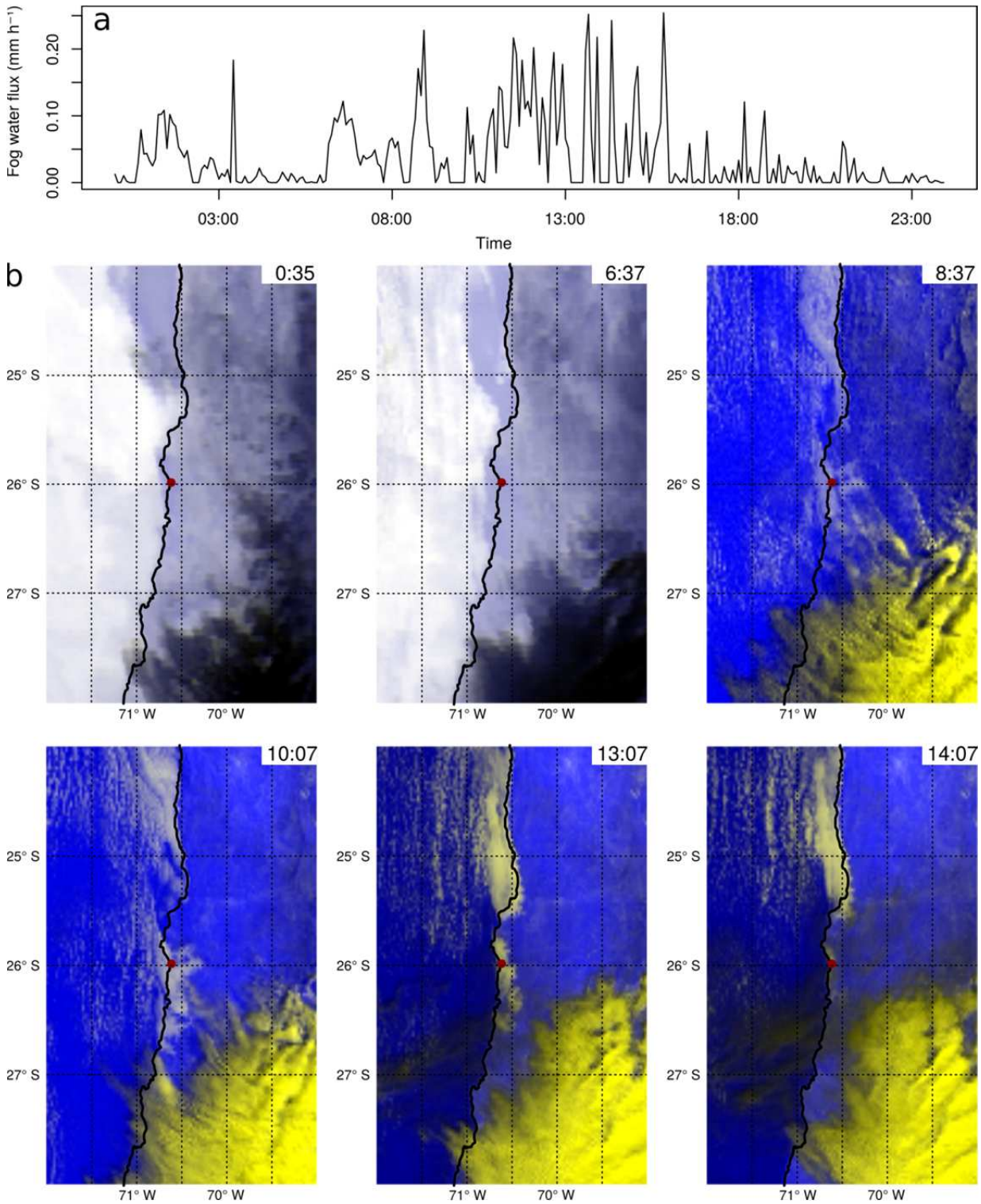

Fig. 6. Fog water collected at the main station (a) and GOES colour composites for April 25, 2016 (b). In (b), fog/LST during night and day is represented with dark gray and whitish colors, respectively. The red circle shows the location of Las Lomitas and the coast is included as the black line. Time of image acquisition given at the top right is local time.

modeling were combined to investigate fog dynamics during selected time periods in the austral autumn in a typical fog oasis in Chile. Local fog water input was driven by both local small scale LST clouds and the well-known stratus deck advected from the Pacific Ocean.

Regarding the small-scale fog events, the modeling approach revealed that katabatic drainage flows during the night converged in the early morning with relatively warm air at the coast leading to local condensation. After sunrise, the wind system changed direction and transported moist

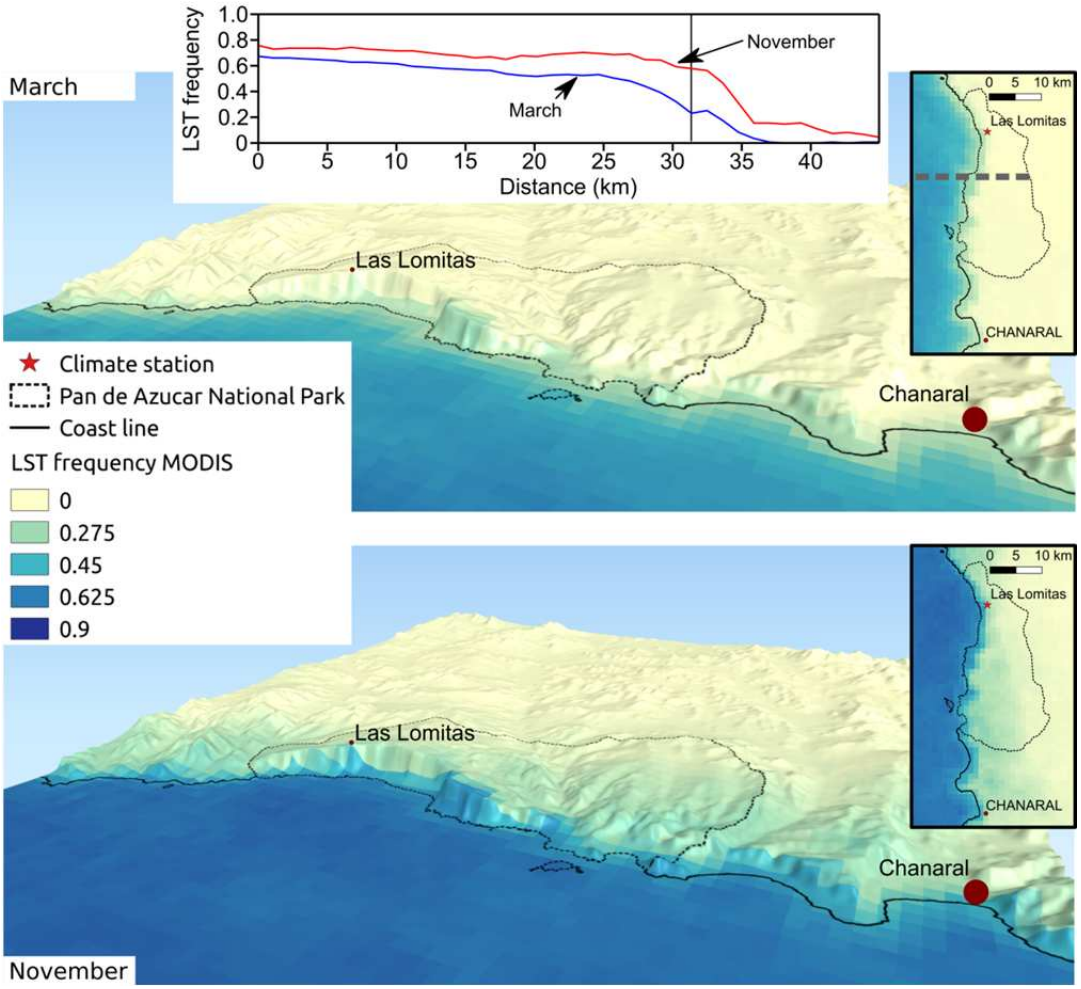

Fig. 7. MODIS average LST frequency for March and November for the period 2010 to 2014 in the area of Pan de Azúcar National Park. The two profiles at the top depict fog frequencies for March (blue) and November (red) along the grey dotted line shown in the small map for March. The vertical line in the profile symbolizes the location of the coastline. Please note that LST frequencies were calculated as the number of overpasses with LST divided by the total number of overpasses in the same period.

air masses toward the inland, again leading to condensation and fog because of the increasing elevation at the coastal mountain ridge. Both processes were accompanied with an inversion that prevented cloud uplift. Therefore, we conclude that the small-scale events at Las Lomitas can be classified as orographic fog.

The large-scale processes such as the extensive status deck were captured well by existing remote sensing products. Those products were extremely helpful in unveiling the large-scale pattern and in understanding the processes leading to large-scale fog events. However, the frequently observed small-scale orographic fog events were not always detected by such broad-scale products because of the problem with the mixed pixels and the bright background of the land surface in the desert. Therefore, new products with higher spatial resolution are required, which can be adapted to the local conditions. In the present article, a first attempt to achieve such high-resolution fog information based on Landsat images is presented. The approach yielded promising results that were in the range of field observations. Because the overflight time of the Landsat satellites is close to noon and the diurnal cycle of fog water input is unpronounced at least in March and April, Landsat images are apparently a good choice for the future development of fog retrieval algorithms. However, it must be stressed that more data, particularly from *in situ* measurements by meteorological stations and vertical fog profiles recorded by drones, are required to develop such fog retrieval.

Overall, fog water flux collected by the artificial fog collector was considerable, even during austral autumn (mean daily sum of 5.3 mm). This flux serves as an important water resource for the local vegetation dominated by BSCs, because a mean daily water amount of 1.4 mm was available to BSCs. This corresponded to approximately 11% of the total fog water flux measured by the artificial fog collector in the range of observations. However, it has to be stated that further research is required to quantify the contributions of the different water sources to the water budget of the BSCs in the Atacama. Because dominated by green algae or green algal lichens BSC are well adapted to

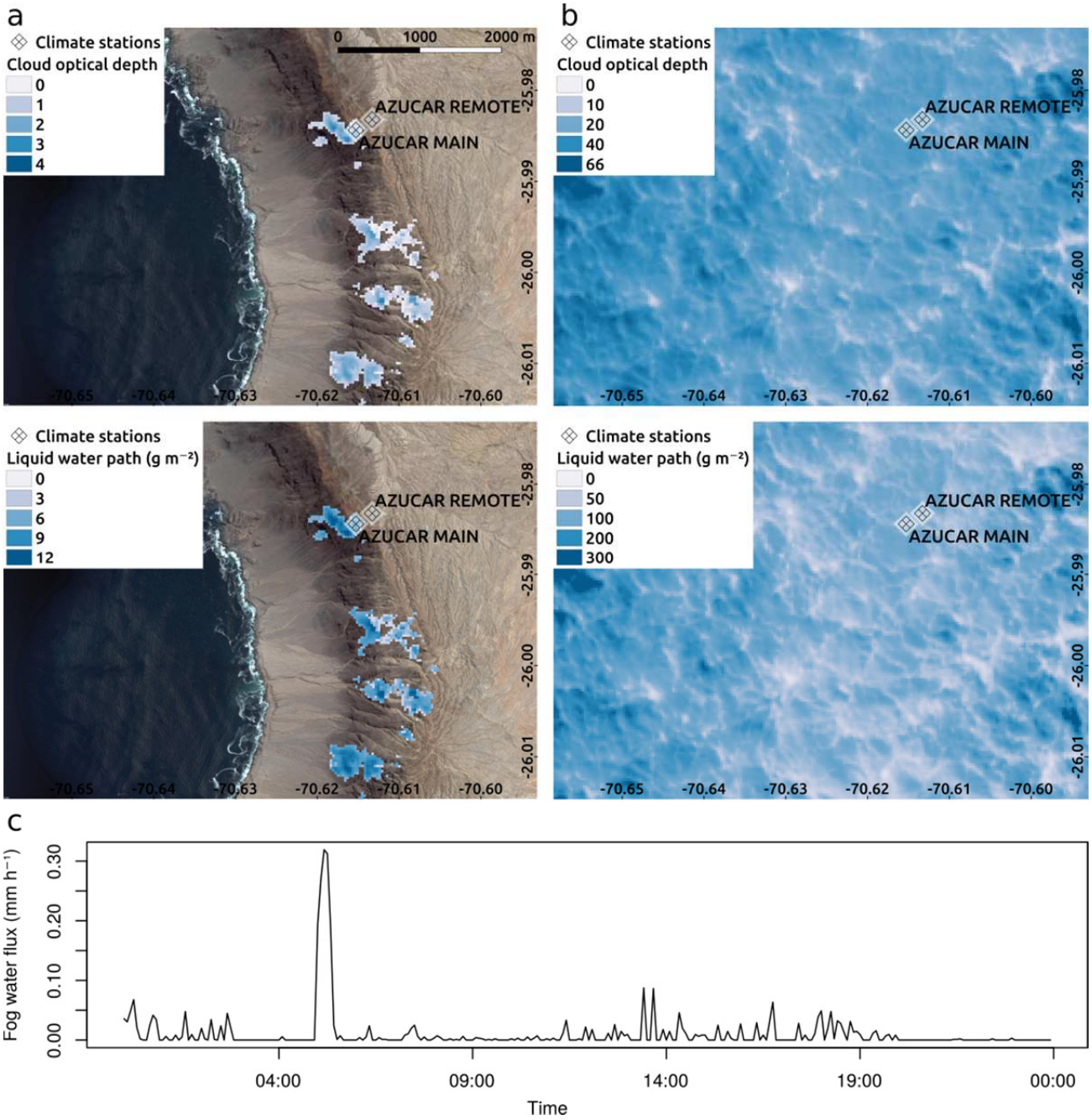

Fig. 8. Landsat-8 cloud based optical depth (COD) and liquid water path (LWP) retrievals in the area of Pan de Azúcar National Park/Las Lomitas for March 10, 2016 (a), and April 11, 2016 (b), at1137 LT each. Time series of fog water flux at the main station for 11 Apr 2016 (c). The low fog water flux measured at the meteorological station at overpass time indicated that either the thick, low stratus deck did not touch the ground or that wind speeds were low.

hyper-arid conditions, even such a low input of water is sufficient for biological activity of BSCs also in other areas of the world (Lange and Redon, 1983; Lange *et al.*, 1994; Colesie *et al.*, 2014, 2016). In the future, to understand the heterogeneous vegetation patterns along the coast and to quantify ecosystem services provided by the local vegetation and particularly the BSCs, comprehensive and spatially explicit information about fog water fluxes in the Atacama will be of great importance.

In the future, the comprehensive analysis of low- and high-resolution satellite products trained and validated against field observations from meteorological stations, cloud microphysics from drone profiles and numerical modeling will allow the spatial analysis of water budgets of BSCs as ecosystem engineers with high spatial resolution. Despite the current lack of data, this case study clearly showed the principle feasibility of our approach combining field measurements, drone profiling, remote sensing and numerical modeling.

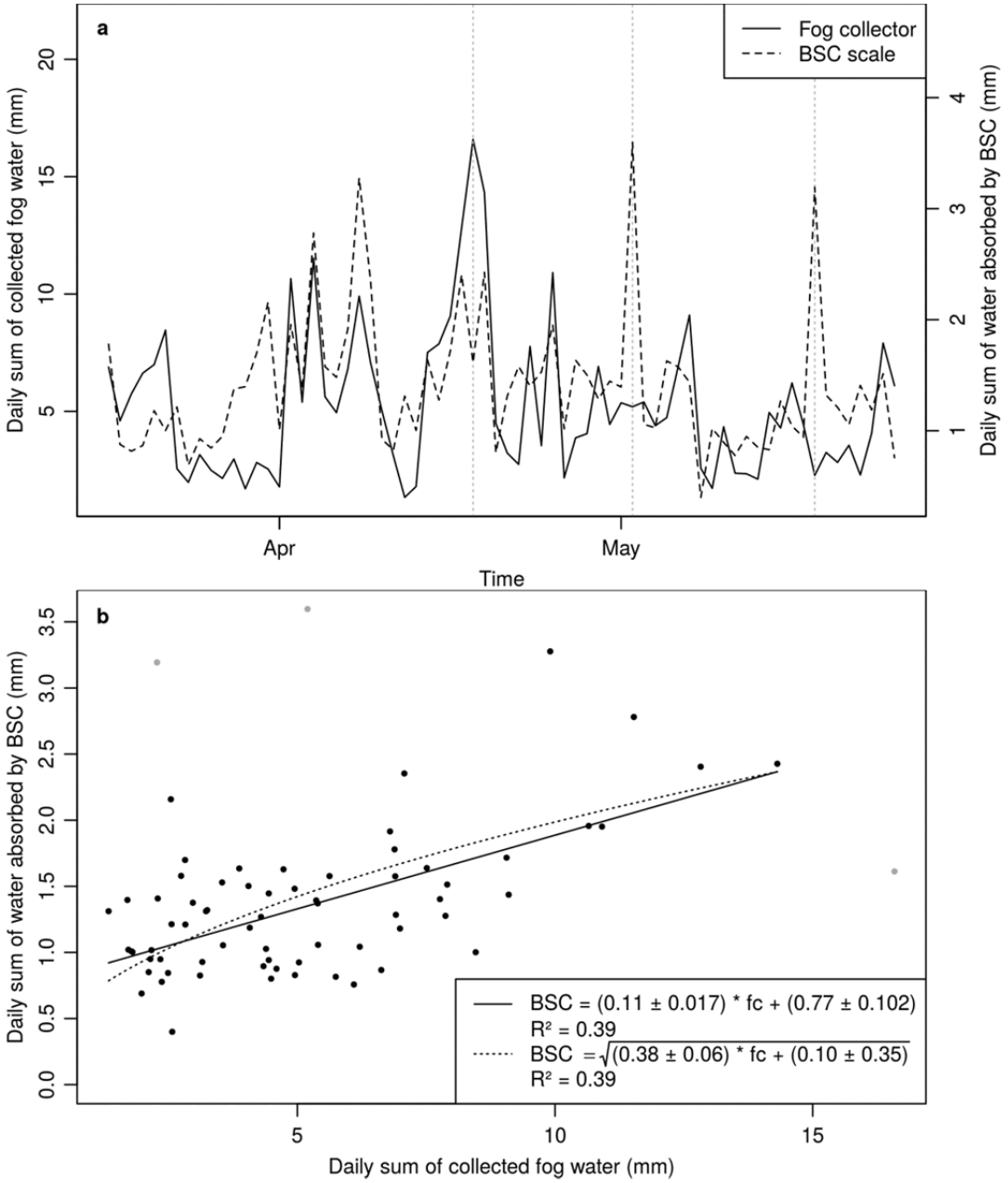

Fig. 9. Time series of daily sums of fog water fluxes (solid line) and water availability to the BSCs (dashed line, a). Scatterplot with the regression lines of the linear (solid) and non-linear (dotted) model between daily sums of water input on the BSC scale and daily sums of fog water fluxes at the fog collectors (b). The three gray data points were treated as outliers in the linear regression analysis. In (a), the outliers are marked by the vertical dotted lines. The equations of the regressions including the standard errors of the estimates and the R^2-value are given at the bottom. In the equations, BSC and fc refer to BSC scale and fog collector, respectively.

ACKNOWLEDGEMENTS

The authors acknowledge financial support from the German Science Foundation (DFG) priority research program SPP-1803 "EarthShape: Earth Surface Shaping by Biota" (project CRUSTWEATHERING: BE1780/44-1, KA899/32-1, BU666/19-1, LE903/14-1). We are also grateful to the Chilean National Park Service (CONAF) for providing access to the sample locations and on-site support of our research.

REFERENCES

Ackerman, S.A., Strabala, K.I., Menzel, W.P., Frey, R.A., Moeller, C.C. and Gumley, L.E. (1998). Discriminating clear sky from clouds with MODIS. *J. Geophys. Res.* 103: 32141–32157.

Angelis, C.F., McGregor, G.R. and Kidd, C. (2004). A 3 year climatology of rainfall characteristics over tropical and subtropical South America based on tropical rainfall measuring mission precipitation radar data. *Int. J.*

Climatol. 48: 385–399.

Belnap, J. and Lange, O. (2001). *Biological soil crusts: Structure*. Function, and Management Springer, Berlin.

Bendix, J. (1995). A case study on the determination of fog optical depth and liquid water path using AVHRR data and relations to fog liquid water content and horizontal visibility. *Int. J. Remote Sens.* 16: 515–530.

Bendix, J. (2002). A satellite-based climatology of fog and low-level stratus in Germany and adjacent areas. *Atmos. Res.* 64: 3–18.

Bendix, J., Thies, B., Cermak, J. and Nauss, T. (2005). Ground fog detection scheme from space based on MODIS daytime data – A feasibilty study. *Weather Forecasting* 20: 989–1005.

Borthagaray, A.I., Fuentes, M.A. and Marquet, P.A. (2010). Vegetation pattern formation in a fog-dependent ecosystem. *J. Theor. Biol.* 265: 18–26.

Bowker, M.A., Belnap, J. and Miller, M.E. (2006). Spatial modeling of biological soil crusts to support rangeland assessment and monitoring. *Rangeland Ecol. Manage.* 59: 519–529.

Castillo-Monroy, A.P., Maestre, F.T., Delgado-Baquerizo, M. and Gallardo, A. (2010). Biological soil crust modulate nitrogen availability in semi-arid ecosystem: Insights from a Mediterranean grassland. *Plant Soil* 333: 21–34.

Cereceda, P. and Schemenauer, R.S. (1991). The occurrence of fog in Chile. *J. Appl. Meteorol.* 30: 1097–1105.

Cereceda, P., Osses, P., Larrain, H., Farias, M., Lagos, M., Pinto, R. and Schemenauer, R.S. (2002). Advective, orographic and radiation fog in the Tarapacá region, Chile. *Atmos. Res.* 64: 261–271.

Cereceda, P., Pinto, R., Larrain, H., Osses, P. and Farías, M. (2004). Geographical description of three fog ecosystems in the Atacama coastal desert of Chile. Third International Conference on Fog, Fog Collection and Dew. Ciudad del Cabo, Sudáfrica.

Cereceda, P., Larrain, H., Osses, P., Farías, M. and Egaña, I. (2008a). The spatial and temporal variability of fog and its relation to fog oases in the Atacama Desert, Chile. *Atmos. Res.* 87: 312–323.

Cereceda, P., Larrain, H., Osses, P., Farías, M. and Egaña, I. (2008b). The climate of the coast and fog zone in the Tarapacá Region, Atacama Desert, Chile. *Atmos. Res.* 87: 301–311.

Cermak, J. and Bendix, J. (2011). Detecting ground fog from space - A microphysics-based approach. *Int. J. Remote Sens.* 32: 3345–3371.

Colesie, C., Green, T.G.A., Haferkamp, I. and Büdel, B. (2014). Habitat stress initiates changes in composition, CO_2 gas exchange and C-allocation as life traits in biological soil crusts. *ISME J.* 8: 2104–2115.

Colesie, C., Green, T.G.A., Raggio, J. and Büdel, B. (2016). Summer activity patterns of Antarctic and high alpine lichen dominated biological soil crusts - Similar but different? *Arctic Antarct. Alpine Res.* 48: 449–460.

Cunningham, P. (2007). Idealized numerical simulations of the interactions between buoyant plumes and density currents. *J. Atmos. Sci.* 64: 2105–2115.

Curatola Fernández, G.F., Obermeier, W.A., Gerique, A., Sandoval, M.F.L., Lehnert, L.W., Thies, B. and Bendix, J. (2015). Land cover change in the Andes of Southern Ecuador—Patterns and drivers. *Remote Sens.* 7: 2509–2542.

Dedieu, G., Deschamps, P.Y. and Kerr, Y.H. (1987). Satellite estimation of solar irradiance at the surface of the earth and of surface albedo using a physical model applied to Meteosat data. *J. Clim. Appl. Meteorol.* 26: 79–87.

Dee, D.P., Uppala, S.M., Simmons, A.J., Berrisford, P., Poli, P., Kobayashi, S., Andrae, U., Balmaseda, M.A., Balsamo, G., Bauer, P., Bechtold, P., Beljaars, A.C.M., van de Berg, L., Bidlot, J., Bormann, N., Delsol, C., Dragani, R., Fuentes, M., Geer, A.J., Haimberger, L., Healy, S.B., Hersbach, H., Hólm, E.V., Isaksen, L., Kållberg, P., Köhler, M., Matricardi, M., McNally, A.P., Monge-Sanz, B.M., Morcrette, J.J., Park, B.K., Peubey, C., de Rosnay, P., Tavolato, C., Thépaut, J.N. and Vitart, F. (2011). The ERA-Interim reanalysis: Configuration and performance of the data assimilation system. *Q. J. R. Meteorolog. Soc.* 137: 553–597.

Dobber, M.R., Dirksen, R.J., Levelt, P.F., van den Oord, G.H.J., Voors, R.H.M., Kleipool, Q., Jaross, G., Kowalewski, M., Hilsenrath, E., Leppelmeier, G.W., de Vries, J., Dierssen, W. and Rozemeijer, N.C. (2006). Ozone monitoring instrument calibration. *IEEE Trans. Geosci. Remote Sens.* 44: 1209–1238.

Egli, S., Maier, F., Bendix, J. and Thies, B. (2015). Vertical distribution of microphysical properties in radiation fogs - A case study. *Atmos. Res.* 151: 130–145.

Elbert, W., Weber, B., Burrows, S., Steinkamp, J., Büdel, B., Andreae, M.O. and Pöschl, U. (2012). Contribution of cryptogamic covers to the global cycles of carbon and nitrogen. *Nat. Geosci.* 5: 459–462.

Falconer, R.E. and Falconer, P.D. (1980). Determination of cloud water acidity at a mountain observatory in the Adirondack Mountains of New York State. *J. Geophys. Res.* 85: 7465–7470.

Fischer, T., Veste, M., Bens, O. and Hüttl, R.F. (2012). Dew formation on the surface of biological soil crusts in central European sand ecosystems. *Biogeosciences* 9: 4621–4628.

Garreaud, R., Barichivich, J., Christie, D.A. and Maldonado, A. (2008). Interannual variability of the coastal fog at Fray Jorge relict forests in semiarid Chile. *J. Geophys. Res.* 113: G04011.

Guyot, G., Gourbeyre, C., Febvre, G., Shcherbakov, V., Burnet, F., Dupont, J.C., Sellegri, K. and Jourdan, O. (2015). Quantitative evaluation of seven optical sensors for cloud microphysical measurements at the Puy-de-Dôme Observatory, France. *Atmos. Meas. Tech.* 8: 4347–4367.

Hong, S.Y., Noh, Y. and Dudhia, J. (2006). A new vertical diffusion package with an explicit treatment of entrainment processes. *Mon. Weather Rev.* 134: 2318–2341.

Jacobs, A.F.G., Heusinkveld, B.G. and Berkowicz, S.M. (2000). Dew measurements along a longitudinal sand dune transect, Negev Desert, Israel. *Int. J. Biometeorol.*

43: 184–190.

Kain, J.S. (2004). The Kain-Fritsch convective parameterization: An update. *J. Appl. Meteorol.* 43: 170–181.

Kalnay, E., Kanamitsu, M., Kistler, R., Collins, W., Deaven, D., Gandin, L., Iredell, M., Saha, S., White, G., Woollen, J., Zhu, Y., Leetmaa, A., Reynolds, R., Chelliah, M., Ebisuzaki, W., Higgins, W., Janowiak, J., Mo, K.C., Ropelewski, C., Wang, J., Jenne, R. and Joseph, D. (1996). The NCEP/NCAR 40-year reanalysis project. *Bull. Am. Meteorol. Soc.* 77: 437–471.

Kriebel, K.T. (1989). Cloud liquid water path derived from AVHRR data using APOLLO. *Int. J. Remote Sens.* 10: 723–729.

Lange, O.L. (1980). Moisture content and CO_2 exchange of lichens. I. Influence of temperature on moisture dependent net photosynthesis and dark respiration in *Ramalina maciformis*. *Oecologia* 45: 82–87.

Lange, O.L. and Redon, J. (1983). Epiphytische Flechten im Bereich einer chilenischen „Nebeloase“ (Fray Jorge) II. Ökophysiologische Charakterisierung von CO_2-Gaswechsel und Wasserhaushalt. *Flora* 174: 245–284.

Lange, O.L., Meyer, A., Zellner, H. and Heber, U. (1994). Photosynthesis and water relations of lichen soil crusts: field measurements in the coastal fog zone of the Namib Desert. *Funct. Ecol.* 8: 253–264.

Larrain, H., Velasquez, F., Cereceda, P., Espejo, R., Pinto, R., Osses, P. and Schemenauer, R.S. (2002). Fog measurements at the site “Falda Verde” north of Chañaral compared with other fog stations of Chile. *Atmos. Res.* 64: 273–284.

Levelt, P.F., Van den Oord, G.H.J., Dobber, M.R., Malkki, A., Visser, H., de Vries, J., Stammes, P., Lundell, J.O.V. and Saari, H. (2006). The Ozone monitoring instrument, *IEEE Trans. Geosci. Remote Sens.* 44: 1093–1101.

Li, J.L.F., Waliser, D., Woods, C., Teixeira, J., Bacmeister, J., Chern, J., Shen, B.W., Tompkins, A., Tao, W.K. and Köhler, M. (2008). Comparisons of satellites liquid water estimates to ECMWF and GMAO analyses, 20th century IPCC AR4 climate simulations, and GCM simulations. *Geophys. Res. Lett.* 35: L19710.

Masunaga, H., Nakajima, T.Y., Nakajima, T., Kachi, M., Oki, R. and Kuroda, S. (2002). Physical properties of maritime low clouds as retrieved by combined use of Tropical Rainfall Measurement Mission Microwave Imager and Visible/Infrared Scanner: Algorithm. *J. Geophys. Res.* 107: AAC 1-1–AAC 1-12.

Muenchow, J., Bräuning, A., Rodriguez, E.F. and von Wehrden, H. (2013). Predictive mapping of species richness and plant species' distributions of a. Peruvian fog oasis along an altitudinal gradient. *Biotropica* 45: 557–566.

Obregon, A., Gehrig-Downie, C., Gradstein, S.R. and Bendix, J. (2014). The potential distribution of tropical lowland cloud forest as revealed by a novel MODIS-based fog/low stratus night-time detection scheme. *Remote Sens. Environ.* 155: 312–324.

Rundel, P.W., Dillon, M.O. and Palma, B. (1996). Flora and vegetation of Pan de Azúcar National Park in the Atacama Desert of northern Chile. *Gayana Bot.* 53: 295–315.

Schemenauer, R.S. and Cereceda, P. (1994). A proposed standard fog collector for use in high-elevation regions. *J. Appl. Meteorol.* 33: 1313–1322.

Schemenauer, R.S., Cereceda, P. and Carvajal, N. (1987). Measurements of fog water deposition and their relationships to terrain features. *J. Clim. Appl. Meteorol.* 26: 1285–1291.

Schulz, N., Aceituno, P. and Richter, M. (2011). Phytogeographic divisions, climate change and plant dieback along the coastal desert of northern Chile. *Erdkunde* 65: 169–187.

Skamarock, W.C. and Klemp, J.B. (2008). A time-split nonhydrostatic atmospheric model for weather research and forecasting applications. *J. Comput. Phys.* 227: 3465–3485.

Stanton, D.E., Huallpa Chávez, J., Villegas, L., Villasante, F., Armesto, J., Hedin, L.O. and Horn, H. (2014). Epiphytes improve host plant water use by microenvironment modification. *Funct. Ecol.* 28: 1274–1283.

Stephens, G.L. (1978). Radiation profiles in extended water clouds. II: Parameterization schemes. *J. Atmos. Sci.* 35: 2123–2132.

Sträter, E., Westbeld, A. and Klemm, O. (2010). Pollution in coastal fog at Alto Patache, Northern Chile. *Environ. Sci. Pollut. Res.* 17: 1563–1573.

Tachikawa, T., Hato, M., Kaku, M. and Iwasaki, A. (2011). Characteristics of ASTER GDEM version 2, Geoscience and Remote Sensing Symposium (IGARSS). 2011 IEEE International Geoscience and Remote Sensing Symposium, pp. 3657–3660.

Tampieri, F. and Tomasi, C. (1976). Size distribution models of fog and cloud droplets in terms of the modified gamma function. *Tellus* 28: 333–347.

Teillet, P.M., Guindon, B. and Goodeonugh, D.G. (1982). On the slope-aspect correction of multispectral scanner data. *Can. J. Remote Sens.* 8: 84–106.

Tewari, M., Chen, F., Wang, W., Dudhia, J., LeMone, M.A., Mitchell, K., Ek, M., Gayno, G., Wegiel, J. and Cuenca, R.H. (2004). Implementation and verification of the unified NOAH land surface model in the WRF model. 20th Conference on Weather Analysis and Forecasting/16th Conference on Numerical Weather Prediction, pp. 11–15.

Thompson, G., Rasmussen, R.M. and Manning, K. (2004). Explicit forecasts of winter precipitation using an improved bulk microphysics scheme. Part I: Description and sensitivity analysis. *Mon. Weather Rev.* 132: 519–542.

Thompson, M.V., Palma, B., Knowles, J.T. and Holbrook, N.M. (2003). Multi-annual climate in Parque Nacional Pan de Azúcar, Atacama Desert, Chile. *Rev. Chil. Hist. Nat.* 76: 235–254.

Trachte, K., Nauss, T. and Bendix, J. (2010a). The impact of different terrain configurations on the formation and dynamics of katabatic flows: Idealised case studies. *Boundary Layer Meteorol.* 134: 307–325.

Trachte, K., Rollenbeck, R. and Bendix, J. (2010b). Nocturnal convective cloud formation under clear-sky conditions at the eastern Andes of South Ecuador. *J.*

Geophys. Res. 115: D24203.

Vermote, E.F., Tanre, D., Deuze, J.L., Herman, M. and Morcette, J.J. (1997). Second simulation of the satellite signal in the solar spectrum, 6S: An overview. *IEEE Trans. Geosci. Remote Sens.* 35: 675–686.

Westbeld, A., Klemm, O., Grießbaum, F., Sträter, E., Larrain, H., Osses, P. and Cereceda, P. (2009). Fog deposition to a Tillandsia carpet in the Atacama Desert. *Ann. Geophys.* 27: 3571–3576.

Wood, R. and Hartmann, D.L. (2006). Spatial variability of liquid water path in marine low cloud: The importance of mesoscale cellular convection. *J. Clim.* 19: 1748–1764.

Zhou, M., Zeng, X., Brunke, M., Zhang, Z. and Fairall, C. (2006). An analysis of statistical characteristics of stratus and stratocumulus over eastern Pacific. *Geophys. Res. Lett.* 33: L02807.

Received for review, January 11, 2017
Revised, October 4, 2017
Accepted, October 6, 2017